IDeAL: IoT-Based Autonomous Aerial Demarcation and Path-planning for Traversing Agricultural Lands

DEBARPAN BHATTACHARYA, Jadavpur University, India
SUDIP MISRA, Indian Institute of Technology Kharagpur, India
NIDHI PATHAK, Indian Institute of Technology Kharagpur, India
ANANDARUP MUKHERJEE, Indian Institute of Technology Kharagpur, India

In this work, we propose an autonomous and on-board image-based agricultural land demarcation and path-planning system – IDeAL (IoT-Based Autonomous Aerial Demarcation and Path-planning for Traversing Agricultural Lands) – using our advanced UAV-based aerial IoT platform. Our work successfully addresses the problem of onboard and autonomous path-planning – which conventional UAV-based systems are not capable of – during standalone operations and without preloaded GPS-markers for flight-path way-points. Our aerial system visually identifies non-electronically and singularly tagged agricultural plots and assesses the enclosing boundaries of the identified plot. Subsequently, an on-board path-planning module autonomously generates GPS-waypoints for traversing the identified plot with minimal overlaps and maximal coverage. Our proposed system exhibits an area coverage efficiency of 95.39% , performs pixel-to-GPS coordinate conversion with an accuracy of 90.35%, and has high agricultural potential in applications such as surveying crop-health conditions, spraying pesticide/herbicides, and others. The proposed system has massive applications in scenarios requiring aerial detection, demarcation, geographical tagging and coverage of an area.

Additional Key Words and Phrases: UAV, Agriculture, Aerial land demarcation

ACM Reference Format:
Debarpan Bhattacharya, Sudip Misra, Nidhi Pathak, and Anandarup Mukherjee. 2019. IDeAL: IoT-Based Autonomous Aerial Demarcation and Path-planning for Traversing Agricultural Lands. 1, 1 (September 2019), 22 pages. https://doi.org/10.1145/nnnnnnn.nnnnnnn

1 INTRODUCTION

This work proposes an autonomous and onboard visual land demarcation and mapping system using an Unmanned Aerial Vehicle (UAV) based Aerial IoT platform. Our work – *IDeAL (IoT-Based Autonomous Aerial Demarcation and Path-planning for Traversing Agricultural Lands)* – primarily focuses on agriculture, which requires easily deployable, usable, and economical solutions. While navigating a UAV to a specific location and getting the aerial images may sound easy and viable, how precisely the UAV reaches a location and performs the assigned task is an essential aspect of any such mission. There are high chances for a UAV to deviate from its expected target location due to errors in the Global Positioning System (GPS) signals received. The UAV may traverse to another field and not the real field due to User Equivalent Range Error (UERE) in GPS coordinates. These errors may arise mainly due to the anomaly in the

Authors' addresses: Debarpan Bhattacharya, Jadavpur University, India, debarpanbhatta123@gmail.com; Sudip Misra, Indian Institute of Technology Kharagpur, India, sudip_misra@yahoo.com; Nidhi Pathak, Indian Institute of Technology Kharagpur, India, nidhipathak002@gmail.com; Anandarup Mukherjee, Indian Institute of Technology Kharagpur, India, anandarupmukherjee@ieee.org.

positional occurrence prediction table, known as the ephemeris of the satellite, timing of the satellite clock, noise in the line of communication between the user and the satellite, which are collectively known as the User Equivalent Range Error (UERE).

In this work, the IDeAL platform is designed to handle the loss of connection to its base station, without compromising the allocated mission. The low-power and intermittent connectivity associated with constrained IoT networks more often come to play during such operations, which can severely hamper the success of missions and even pose a threat to lives or infrastructure during a loss of connection. The proposed platform is designed to handle such situations. Each UAV used in the IDeAL platform acts as an enabler for Agricultural IoT. The land demarcation process includes aerial imagery, acquisition of GPS location, generating a waypoint map for the demarcated field and land traversal. These data are further used for tracking and record keeping, determining the status of the field and for performing further missions. Moreover, each UAV is a complex system in itself which involves heterogeneous data acquisition from its on-board sensors. The IDeAL platform is initially approximately directed to a zone of interest. The system visually locates and identifies a plot/plots of interest based on the presence of a non-electronic ground marker/beacon. This simple marker helps the UAV identify its owner's plots, and separate them from other plots. Upon identification, the onboard modules access the boundaries of the plot of interest, estimates GPS markers for the plot corners/edges directly from its current location, altitude and aerial image of the identified plot. Upon establishing the GPS bounds of the plot, the UAV's onboard module creates a set of GPS waypoints for the traversal path within the identified plot to ensure maximum non-overlapping coverage. The efficiency of the proposed system lies in accurate detection of the GPS coordinates of the target field and maximum coverage of the target area. Fig.1 shows the overview of the proposed system.

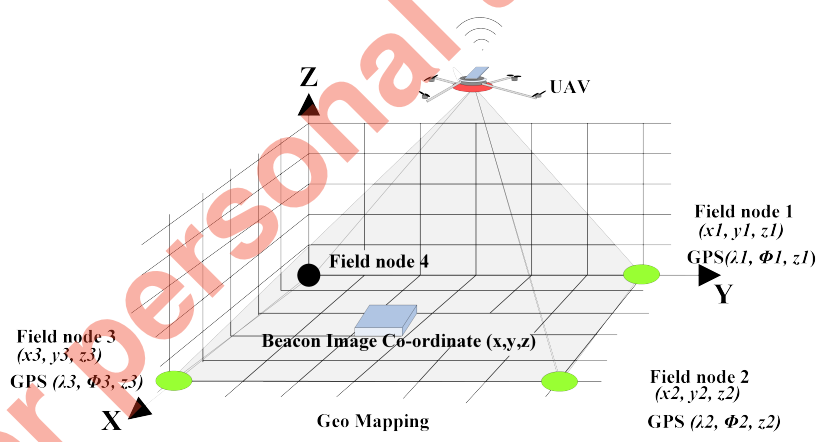

Fig. 1. Geo mapping of enclosed field

1.1 UAVs in Remote Sensing

Application of UAVs in aerial remote sensing and land mapping is a progressive field of research, which has great potential in various applications such as detecting an unknown part of an island based on only GPS information followed by visual mapping of the land. Currently, UAVs are being used for various applications, which includes monitoring crop-health in an agricultural field, taking care of the rate of yield and diseases of crops, disaster management in critical

environmental condition, making high-resolution aerial imagery of a field using UAV mounted with high-resolution cameras, which is not available in the satellite-based image. Spectrum specific cameras are used in UAVs to target vegetations, different landforms, and crops for their detection and analysis. UAVs with LiDAR and hyperspectral imagery are used to detect the type of vegetation and plant species[16]. Aerial images have also been used for boundary delineation and updating cadastral maps with the help of image processing[5]. Recently, a study suggested the use of UAVs in land delineation for land registration purpose using UAV acquired images in Indonesia[15]. Urban planning and land usage estimation have also found extensive use of UAVs to help get a complete 3D view-based approximation of an area of interest. The UAV-based method not only reduces the time and human resources required but also provides more reliable and accurate data[12][6].

For agricultural purposes entailing issues of plot ownership, UERE becomes more prominent in case of small-scale fields, especially in India, where a majority of the agricultural land holdings are small and fragmented. In 2002-2003 the average Indian farmland size was 1.06 hectare. Moreover, every holding is distributed in several sub-holdings. Therefore, a small percentage error in UAV repositioning significantly affects the coverage for smaller fields. A small error in the geographical location can divert the UAV from its target location resulting in partial or complete loss of desired information. The orientation of the camera mounted on the UAV also effects the area covered under the mission. These errors are inevitable but can be handled with pre-programmed correction measures. Table1 shows the notations that

Table 1. Notations used in this paper and corresponding significance

Symbolic Notations	Significance
M=M_xxM_y	Original Marker Size
M_i	Marker Occupancy in image
δ_m	Error in Area of Detected Marker
H	Altitude of UAV
β	Diagonal Field of View (DFoV) of the Camera
pxq	Pixel-Resolution of Image-Sensor of the Camera
I_m(x,y)	Detected contour of Marker
M_{ab}	Image Raw Moment of Marker
M_c(x,y)=(C_x,C_y)	Centroid of Marker
R_{marker}	HSV Range for Marker Detection
A_{marker}	Area of the Detected Contour of Marker
$A_{BoundaryThreshold}$	Threshold Area of the Contour of Detected Target Boundary
I_{pxq}	Image Captured from UAV of resolution pxq
V_{thr}	Grayscale Threshold for Target Boundary Detection
S_{field}	Contour of Target Field Boundary
H_{field}	Convex Hull form of Target Field Boundary
W_{field}	Image Waypoint-map for Target Land Coverage
d_s	Image-sensor Footprint Width
D_s=d_s-δ_s	Perpendicular Drift of UAV during Field Coverage where δ_s represents overlap
T_{field}	Strips evaluated from H_{field} for path coverage
D_R	Real Distance of Image Distance d_i
f	Focal length of the camera
ρ_p	Pixel Density of the Image sensor
(ϕ_b, λ_b)	Corresponding latitude and longitude of (C_x, C_y)
R	Radius of Earth

will be further used throughout the paper.

1.2 IDeAL for Path Planning

The IDeAL system aims to detect a specific field of interest and create a geo-map to explicitly define the target field, geographically. This geographic division is followed by an efficient path planning to ensure complete coverage of the detected field with maximal non-overlapping coverage. Before this, an approximate GPS location of the field/plot is input to the UAV such that it flies to the given location and captures images of the plot. In cases of smaller plots such as the ones typically found in developing countries like India, the UERE is unacceptable. Considering the GPS error, it may happen that the location may or may not lie inside the targeted field, which may cause the UAV to monitor someone else's plots.

To ensure that the field is selected correctly, a non-electronic marker is placed inside the field in any arbitrary location. The UAV-mounted camera captures the images of the field and processes it onboard its secondary processor. This process continues until the marker placed inside the field is detected. After successful detection of the marker, the image is further processed to detect the enclosing boundary of the marker, which is the field/plot area. Fig. 2 outlines the steps followed by an UAV during execution of IDeAL. An efficient path planning is required for complete coverage of the field, satisfying optimum solution for parameters pertaining to good path planning. We additionally propose a path planning approach – *Strip Division along Resultant Wind Flow (SDRWF)*, which ensures minimum loss of information, less coverage time, smaller distance traversed by UAV, and lower probability of deviation of UAV from the defined path.

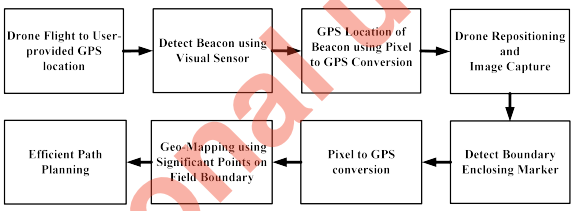

Fig. 2. Sequence of operations followed by the UAV during execution of IDeAL.

1.3 Motivation

The presence of UERE in low-cost, off-the-shelf GPS receivers makes it challenging regular UAVs to precisely locate target points with minimal errors. For the accurate detection of the target field, the UAV should reach the user provided GPS location correctly, especially in case of small land holdings. Offline methods to detect and delineate land using aerial imagery [5] take time and may require multiple missions to achieve the land traversal with high accuracy. Vision-based traversal requires continuous imagery and processing to decide the path of the UAV which adds computational overhead to the UAVs on-board processor[1]. In case of detection of a real target field, the shape that is detected generally has many concave curvatures. Jiao *et al.*[10] simulate a process for implementing path planning on a concave polygon. However, in a real-life scenario, their approach is challenging to be implemented due to the presence of the concave curvatures as stated by Araujo *et al.* [2]. Parameters such as loss of information, distance traversed by UAV, energy consumption, number of sharp turns, and others are of significant concern in the existing path planning approaches. The proposed approach tries to address the mentioned issues efficiently with the following points of motivation:

- Presence of UERE in GPS coordinate of the marker makes it difficult for the UAV to locate the target field accurately.
- The UAVs are not capable of designing geo-map for the field and develop an efficient path planning process onboard and autonomously in the existing approaches.
- The existing approaches are not capable of exclusively generating GPS way-point map directly after the demarcation process is performed on the images. They typically have to rely on external systems and computing platforms for generating the waypoints.
- Existing approaches have limitations of adequate coverage due to the existence of sharp turns for UAVs, loss of information, and flight time.
- Real-time detected fields have various concave curvatures and complexity which make path planning non-trivial.

1.4 Contribution

In the proposed approach, the probability of GPS repositioning errors due to UERE is avoided using UAV position confirmation and ground marker detection. The probable error in target field detection due to the visibility of multiple fields from UAV image sensors is addressable by detection of the enclosing boundary of the marker only. Generally, the detected boundary of the target field is a complex polygon having many edges and corners as well as many concave curvatures. Eventually, the system converts the detected polygon to its convex hull, after which a path planning algorithm is applied on the convex field considering the resultant wind velocity direction. The ensuing path planning is such that the path generated is parallel to the wind direction to reduce the deviation of UAV from its path. The pixel way-points generated from the plot/field's image are converted to GPS way-points for real-time coverage of the target field. The proposed approach offers the following contributions considering the issues of real-time performance guarantees with the present approaches and the motivation mentioned in the previous section:

- A marker-based approach for detection and demarcation of a target field to avoid the GPS error due to UERE.
- An efficient contour adaptive path planning approach on the processed image.
- An algorithm for the image way-point to GPS way-point conversion, as stated in Algorithm 3, with an accuracy of 90.35%.

  The only prerequisite for the system is the approximate GPS location of the target land. The system guides the rest of the process.

1.5 Paper Organization

The work in this paper is organized as follows. Section 2 includes discussions about some related works on field demarcation using UAV with various types of sensors and path planning approaches to cover the whole target field efficiently. Subsequently, Section 3 describes the system architecture used along with the algorithms and mathematical formulations. This is followed by Section 4, which includes the experimental results achieved and the analysis of its performance. Finally, Section 5 concludes the paper with some proposed future works to gain better accuracy and make the approach more robust.

2 RELATED WORKS

The approach discusses the development of a full setup for effective detection of enclosing boundary of an agricultural field followed by path planning. The same system is rigorously usable for purposes where the prime concern involves

demarcating and traversing a specific area of interest. On-board decision-making system for UAVs has been a generic approach to observe the conditions of an area of interest and initiate appropriate action. Using aerial imagery as a mode to detect various health conditions of the crops, their growth rate and the field has been a prime area of interest. Alsalam *et al.* has implemented this in [1] using the Observation, Orientation, Decision, and Action (OODA) based loop framework. Similarly, ortho-rectified aerial images have been used to analyze the relationship between the height and health condition of crops[11][8]. UAVs have also been used in coordination with ground wireless sensor networks (WSN) to provide on-demand services to the agricultural fields[4].

Traditionally, the vegetation index computed from the aerial images from satellites has been used to detect overall health and the surrounding environmental conditions. In the present-day, UAVs effectively take care of these operations at a much higher spatiotemporal resolution, that too at a fraction of the cost required for satellite-based imagery. Indices such as Normalized Difference Vegetation Index (NDVI), Normalized Difference Water Index (NDWI), and Soil-adjusted Vegetation Index (SAVI) indices were used to determine the denser and lower vegetation area, water content and overall health condition of the crop in [18]. A similar approach is used in [17] where the authors have analyzed the aerial images of multi-spectral bands (red, green, NIR channel) using different linear and logarithmic regression models to monitor rice plant health. Feature detection techniques were used for low-altitude mapping using camera-equipped UAV in [13].

Path planning using UAV is one of the fields that has gathered much attention from the researchers. It plays a significant role in the efficiency of a task being performed by a UAV. The major challenge is to ensure the complete coverage of the area of interest, avoiding any loss or unwanted coverage of the area. Since the contour of an area is generally polygonal and not uniform, any approach needs proper planning and calculation. An improved exact cellular decomposition method is proposed in [10], which applies to polygonal areas for coverage planning. Optimal coverage by concave to convex polygon conversion is proposed in [2], giving a comparative analysis of different path planning approaches. Real-time computation of the path and mapping has been addressed in [9] through frequency-based contextual classification of both spectral and spatial information of digital aerial images. However, the approaches mentioned do not consider the deviation in UAV's trajectory due to environmental conditions. A highly efficient and stable UAV can reduce this effect and maintain the efficiency of path planning. Artificial Neural Network (ANN) and Particle Swarm Optimization (PSO) were proposed to stabilize UAV operations in a changeable environmental situation [7].

2.1 Synthesis

Aligning with the current research work, this paper focuses on using aerial imagery to detect and demarcate an agricultural piece of land along with an efficient path planning technique. The method takes into account the environmental conditions and its effect on the UAV's trajectory. Although it has been demonstrated in terms of the agricultural usage, the generalized path planning model that can be used for various purposes, not just limited to agricultural fields.

3 AERIAL MONITORING PLATFORM

The aerial IoT platform for the IDeAL system consists of a four-rotor UAV, which wirelessly links to a ground control station for initial controls and subsequent monitoring of flight. The UAV consists of primary and secondary processors. The primary processor, which we also refer to as the flight controller board, is responsible for the control and operation of the UAV. The primary processor integrates a gyroscope, internal compass, barometer, and a suite of other sensors to keep the aerial platform airborne and operational. A regular USB camera connects to the UAV system's secondary

processor. The secondary processor is also responsible for processing and onboard decision making. Fig. 3 outlines the major functional blocks of the aerial platform.

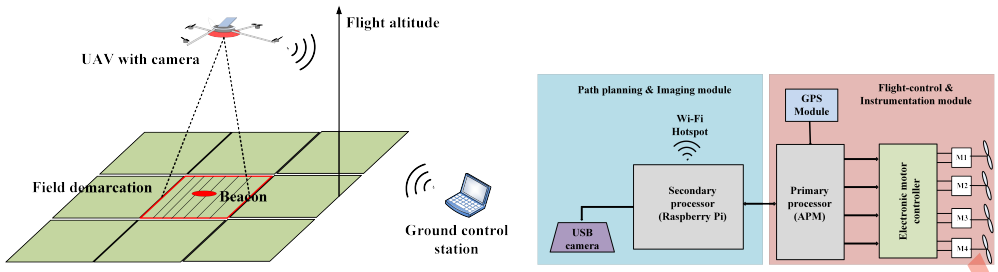

(a) Basic IDeAL operation (b) Block diagram of the UAV

Fig. 3. The proposed aerial IoT-based land demarcation system.

The algorithms designed for the marker demarcation and path planning are executed in the secondary processor. This processor also oversees and controls the wireless communication between the UAV and the ground control station. A WiFi access point is created using the secondary processor, which is used to connect to the ground control station, which initiates the UAV's mission. This access point enables the ground control station to connect to the UAV during its mission. The ground control station connects to the UAV and initiates the mission using the programmed scripts in the secondary processor of the UAV. The data processed by the UAV are sent continuously to the ground control station, which enables real-time monitoring of UAV during the mission. Fig. 3(a) depicts the connection outline of the system during its operation.

4 METHODOLOGY FOR VISUAL DEMARCATION OF PLOTS

The methodology for visual demarcation of plots using an aerial imaging platform consists of five major parts – 1) marker detection, 2) field boundary estimation, 3) path planning within the target area, 4) marker geo-tagging, and 5) pixel-based waypoint map generation.

Initially, the UAV platform is fed with a GPS location of the target plot by the user. However, due to the significant effect of UERE for small land holdings, the initially fed GPS location is considered as the approximation of the target for the UAV. This presence of UERE restricts the implementation of pre-determined waypoint-based field coverage paths in the UAV. Once the UAV reaches the user-provided GPS location, the UAV attains a specific altitude and starts the process of accurately localizing and verifying the identity of the plot by locating a manually pre-placed blue marker in the target field. Once the marker is detected, the UAV captures the images of the reached field, where it starts estimating the bounds of the field, which is then followed by geographic tagging of the bounds and the subsequent path planning within these bounds. Fig. 4 shows the operational stages of the visual identification and path planning within the identified field. We consider a UAV situated/hovering at an altitude H, which captures image from its camera having a focal length f, diagonal field of view β, and pixel resolution $p \times q$. This work is based upon the assumptions 1 and 2.

Assumption 1. *The plane of the UAV, while in operation, is parallel to the ground.*

Assumption 2. *- All points on the ground are assumed to be zero altitude points, as the unevenness of the ground is negligible compared to H.*

Equation 1 gives the relation between the pixel and real distance in the image.

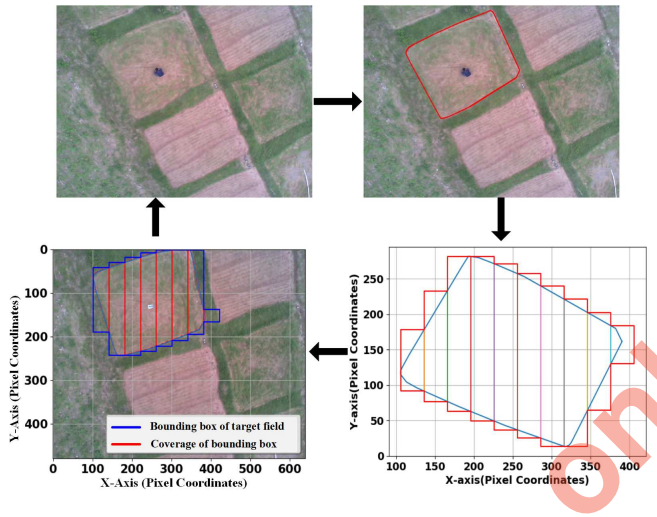

Fig. 4. Geo-mapping and efficient path planning of target-land

The real distance between two pixel coordinates (x_1, y_1) and (x_2, y_2) is given by

$$D_r = \frac{2H\sqrt{(x_1 - x_2)^2 + (y_1 - y_2)^2}\tan(\frac{\beta}{2})}{\sqrt{p^2 + q^2}} \tag{1}$$

as referred in the Fig. 5.

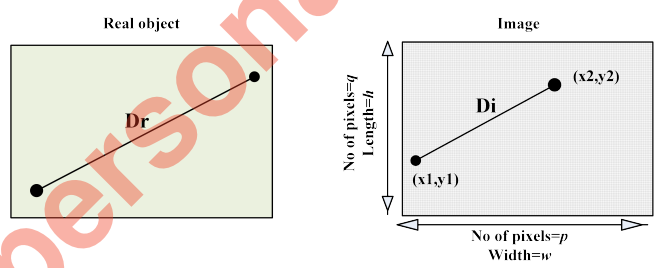

Fig. 5. Image distance to real distance conversion

Considering the diagonal length of the camera lens as d, the relation between β, d and f is represented as:

$$d = 2f\tan\frac{\beta}{2} \tag{2}$$

Subsequently, the pixel density of the image is expressed in relation to an arbitary d_i as

$$\rho_p = \frac{\sqrt{p^2 + q^2}}{d} \tag{3}$$

such that,

$$d_i = \sqrt{(x_1 - x_2)^2 + (y_1 - y_2)^2} \tag{4}$$

Finally, the real distance between two pixel coordinates D_r is expressed using the convex lens formula for image formation as:

$$D_r = \frac{H}{f} D_i = \frac{H}{f} \frac{d_i}{\rho_p} \tag{5}$$

Substituting values from Equations 2, 3, and 4 gives the final Equation 1.

4.1 Marker Detection

The pre-placed blue ground marker in the image is detected using image processing and computer vision tools. The detection process is fast enough to be done proficiently on Raspberry Pi like processor board (the secondary processor of the UAV) mounted on UAV. Thus, the detection process takes place in real-time, while the UAV is on a mission, hovering over the target field. The marker detection algorithm is as in Algorithm 1. The color of the marker is selected

Algorithm 1 Ground Marker Detection

Inputs: Image $\rightarrow I_{p\times q}$ ▹ %$p \times q$ = pixel resolution of the image%
Output: Pixel centroid of marker $\rightarrow M_c(x, y)$
Initialize Parameters:
$U_{cnt} \rightarrow 0$ ▹ %Contains all contours%
$A_{cnt} \rightarrow 0$ ▹ %Area of a contour%
$M_i \rightarrow$ Range of Marker Occupancy ▹ %M_i defined in eqn.1%
$R_{marker} \rightarrow (b_{low}, b_{high})$ ▹ %Marker HSV range%
convert $I_{p\times q}$ from BGR to HSV colorspace $H_{p\times q}$ ▹ %HSV colorspace%
Apply R_{marker} on $H_{p\times q}$ to get detection mask M_{marker}
Noise removal using morphological transformations on M_{marker}
Extract contours from $M_{p\times q}$
Store contours in U_{cnt}
for *cnt* in U_{cnt} **do**
  if ($A_{cnt} \in M_i$) **then**
    Evaluate $M_c(x, y)$ for cnt using equations8 and 9
  else
    reject contour
  end if
end for

to be blue, as this color has the maximum visibility and is easily detectable, especially in agricultural fields with a dominant presence of green and brown colors. We use the HSV color space range for blue color for the detection of the ground marker. There may be some other blue colored object inside or close to the target field, leading to false detection of the marker. We avoid this false detection of other blue objects inside the target boundary by the use of a range of occupancy of the marker in the image and define it such that M_i is the calculated area of the marker in the image (in pixels). For M being the actual area occupied by the marker in the field and for a real-time error consideration δ_m , we formulate the relation in Equation 6 as,

$$M_i \in (M[\frac{\sqrt{p^2+q^2}}{2H\tan(\frac{\beta}{2})}]^2 - \delta_m, M[\frac{\sqrt{p^2+q^2}}{2H\tan(\frac{\beta}{2})}]^2 + \delta_m) \tag{6}$$

After the detection of the marker contour, we calculate the pixel centroid of the marker. If $I(x, y)$ is the pixel function which defines the detected marker, then the raw image moment M_{ab} of the field is defined by Equation 7 as,

$$M_{ab} = \sum_{x=1}^{p}\sum_{y=1}^{q} x^a y^a I(x, y) \tag{7}$$

Subsequently, the centroid coordinate of the marker (C_x,C_y) is defined [14] as,

$$C_x = \frac{M_{a=1,b=0}}{M_{a=0,b=0}} \tag{8}$$

and

$$C_y = \frac{M_{a=0,b=1}}{M_{a=0,b=0}} \tag{9}$$

4.2 Field Boundary Estimation

After the successful detection of the ground marker, we detect the boundary enclosing the marker as described in Algorithm 2. The algorithm detects the enclosing boundary by thresholding of the image. However, in real case scenarios, the detected boundary comes out as a very complex polygon with hundreds of edges and concave curvatures due to distortion, which is not the exact shape of the field. Implementation of path planning using an Improved Exact Cellular Decomposition (IECD) scheme for concave polygons [10] is complicated and time-consuming [2]. So, the convex hull of the detected polygonal boundary is evaluated to get both the exact shape of the field as well as to remove the concave curvatures.

A convex hull is an improved polygon to remove concave portions of a polygon containing a set of points S. It is the intersection of all the convex polygons enclosing S. For finding the convex hull, all points p_i in S are assigned a weighted value γ_i such that sum of γ_i for all p_i is unity. For each combination of γ_i, one point P_{convex} is obtained that lies on the convex hull. For all combinations of γ_i, all points on the hull are achieved, which we mathematically represent as,

$$P_{convex} = \sum_{i=1}^{N(S)} x_i \gamma_i \quad for\ 0 \leq \gamma_i \leq 1\ and \sum_{i=1}^{N(S)} \gamma_i = 1 \tag{10}$$

As the marker has different color gradients compared to the color of the land, sometimes the marker itself is detected as the enclosing boundary. To avoid this probable error, the pixel occupancy of the marker, M_i in the image is calculated using the marker detection algorithm. The lower threshold for occupancy of the detected boundary is set to M_i to avoid false detection of the marker as the boundary. The threshold is given as

$$A_{BoundaryThreshold} = M_i + \delta_b \tag{11}$$

such that δ_b comes from real-time error consideration. The relation between real and the pixel area of the target field is derived using Equation1 as,

$$A_{field} = A_p[\frac{2H\tan(\frac{\beta}{2})}{\sqrt{p^2+q^2}}]^2 \tag{12}$$

The actual areas of the trial fields are measured using a measuring tape, and the efficiency of detection is compared using Equation 12 in the result section.

Algorithm 2 Target Boundary Detection and Path-Planning

Inputs: Image $\rightarrow I_{p\times q}$ ▹ $\%p \times q$ = pixel resolution of the image%
Output: Pixel way-point map for UAV$\rightarrow W_{field}$
Initialize Parameters:
  $count \rightarrow 0$
  $V_{thr} \rightarrow$ pixel threshold for boundary detection
  $B_{p\times q} \rightarrow$ Gray-scale image
  $T_{p\times q} \rightarrow$ Image after apply thresholding
  $U_{cnt} \rightarrow$ store all contours of the boundary
  $S_{field} \rightarrow$ Countour satisfying equation 11
  $H_{field} \rightarrow$ Convex hull of the contour
Convert $I_{p\times q}$ to binary image $B_{p\times q}$ ▹ %grayscale colorspace%
Apply V_{thr} on $B_{p\times q}$ to get $T_{p\times q}$
Noise removal using morphological transformations on $T_{p\times q}$
Extract contours from $T_{p\times q}$
Store contours in U_{cnt}
for *cnt* in U_{cnt} **do** Evaluate S_{field} for cnt
  if $M_c(x, y)$ is inside S_{field} **then**
    $TargetField \rightarrow S_{field}$
    $S_{field} \rightarrow H_{field}$ ▹ S_{field} to H_{field} conversion using equation10
    $H_{field} \rightarrow W_{field}$ ▹ H_{field} to W_{field} conversion using equations14,15,16,17.
  else
    reject cnt
  end if
end for

4.3 Path Planning Within Target Field

After calculating the convex field boundary, S_{field} of the target field, the path for the UAV is calculated. An efficient path planning approach should be able to minimize the field traversal distance, coverage, and energy consumption of a UAV. This strategy reduces the flight time and thus lowers energy consumption. Sharp turns during flight may lead to incomplete coverage of the target field. Hence, sharp turns should be avoided for efficient coverage. Complete area coverage is one of the important aspects of efficient path planning. It not only focuses on covering area inside the target field, but also on avoiding any region outside the field. The parameters defining an efficient path planning approach can be summarized as follows:

- *Distance Traversal:* The UAV should traverse as small a distance as possible to cover the field. This parameter is necessary to reduce the time of operation as commercially available off-the-shelf UAVs are not capable of enduring long-duration flight. This is an import aspect for ensuring balanced energy consumption.
- *Minimum Number of Turns*: As the UAV missions are carried out using GPS way-point maps, there may be sharp turns while traversing the field using the way-point maps. Also, due to the high degree of freedom while in the air, the UAVs suffer tilts and turns. This leads to a loss of some field information during the mission. So, the number of turns should be minimized for efficient path planning.
- *Efficient Area Coverage:* It should be ensured that the whole field is covered without any loss of information as well as no extra information, i.e., the region outside the target field should not be covered. Thus, an efficient area coverage refers to complete field coverage – without any coverage of the field outside the target field.

For the parameters described, we observe during actual field trials that all the parameters cannot be fulfilled at the same time. This restriction means that there has to be a trade-off between the parameters mentioned above while designing a path planning approach. There are some existing path planning approaches discussed in [2] for polygonal fields. We discuss some implementations of the existing approaches and graphically outline them in Fig. 6.

- **Zigzag along Optimal Sweep:** In this approach, the target field is covered very efficiently. The area covered outside the target field is negligible. It sweeps along the width of the polygon; so, it goes through less number of sharp turns [2]. On the other hand, all the turns occur inside the target field as shown in Fig.6(a). So, the probability of losing information is high in this approach.

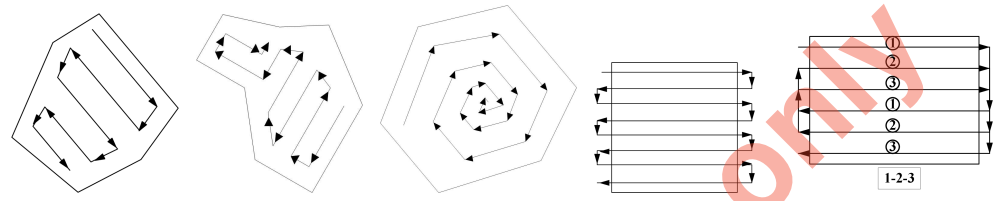

(a) Zigzag along Optimal Sweep (b) IECD (c) Spiral-like Approach with Width Consideration (d) Lawnmower Approach (e) Zambomi Approach

Fig. 6. Path-planning using existing approaches

- **IECD:** In this case, polygons having concave curvatures are divided into convex polygons, and then, for each segmented polygons, path planning is applied along optimal sweep direction[10]. Generally, real fields are detected as a very complex polygon with hundreds of concave curvatures. A scenario may arise that the sensor footprint d_s is greater than the width of a segmented polygon; path planning cannot be implemented in such a scenario. In this case, the number of turns is optimally reduced but all turns occur inside the polygon, as shown in Fig.6(b), which increases the chances of losing information due to tilting of UAV during sharp turns.
- **Spiral Like Approach with Width Consideration**: In this approach, the width of a polygon is evaluated, and the field is covered by spiraling inside the polygon[2]. The turns in the polygon are taken as straight paths rather than curves as in a typical spiral. Due to the sharp nature of the turns, some portion of the area is left uncovered by the UAV during the path planning. Hence, this has to be covered separately. It is clear from Fig. 6(c) that the complexity of this method increases in case of polygons with a large number of edges.
- **Lawnmower Approach:** In this approach, no turns occur inside the target field, thereby decreasing the chances of losing information. However, it covers a comparatively larger distance than previous approaches to make turn outside the field. Lack of time and energy efficiency are the major limitations of this approach [2]. The number of turns can be decreased by carefully choosing the sweep direction with a minimum number of turns to cover an area. Also, this approach restricts multiple visits to the same area. The approach is depicted in Fig. 6(d)
- **Zamboni Approach:** This approach, as shown in the Fig.6(e), is similar to the lawnmower approach, but covers the area that remains uncovered during the turns. Thus, this approach outperforms the lawnmower approach in terms of coverage. Here, the UAV first traverses along path 1, then circulates and goes through path 2, and finally goes through path 3. The distance covered by the UAV in this approach is quite high; although, the probability of losing target information is very low in this case[2].

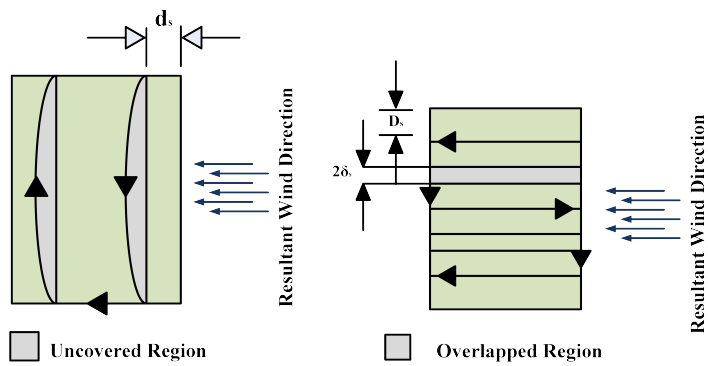

(a) Some region remains uncovered for wind thrust on UAV

(b) Sweep parallel to wind direction causes low deviation and some overlap ensures full coverage

Fig. 7. Advantage of taking sweeps parallel to wind direction

The path planning of the UAV is determined efficiently such that the UAV can cover the field with minimum energy and deviation. The existing approaches emphasize the minimum time consumption and the minimum number of turns for UAVs to efficiently cover the field. However, under the effect of strong wind flows, UAVs are bound to deviate from the planned path, and the field will not be covered efficiently.

In our proposed approach, the effective reduction in deviation of UAV from its designed path is demonstrated in Fig. 7. There is a deviation of UAV in Fig. 7(a), but not in Fig. 7(b). Our proposed *Strip Division along Resultant Wind Flow (SDRWF)* technique is applied for both low time consumption as well as low deviation of UAV. In SDRWF, the polygonal field is divided into strips of width D_s, and is defined as,

$$D_s = d_s - \delta_s \tag{13}$$

Here, d_s is the width of the sensor footprint, δ_s is inserted to ensure some overlap of sensor footprint during path traversal of UAV. This minimal overlap ensures efficient coverage of the field even in severe wind conditions. The benefit of taking sweep directions parallel to the wind direction is shown in the figure. The SDRWF on a polygon is shown in Fig. 8. The detected boundary of the target field is represented by polygon S_{field}. Then S_{field} is converted into convex hull H_{field}. H_{field} is oriented in a clockwise direction starting from the point having the minimum abscissa of all vertices.

$$\begin{aligned} H_{field} &= \{(x_1, y_1), (x_2, y_2), (x_3, y_3)....., (x_n, y_n)\} \\ x_{min} &= min\{x_1, x_2, x_3, \ldots, x_n\} \end{aligned} \tag{14}$$

The whole polygon is divided into strips of width D_s along the resultant wind flow direction. The strips defined by set T are expressed as,

$$T = \{T_1, T_2, T_3, .., T_i, ..\} \tag{15}$$

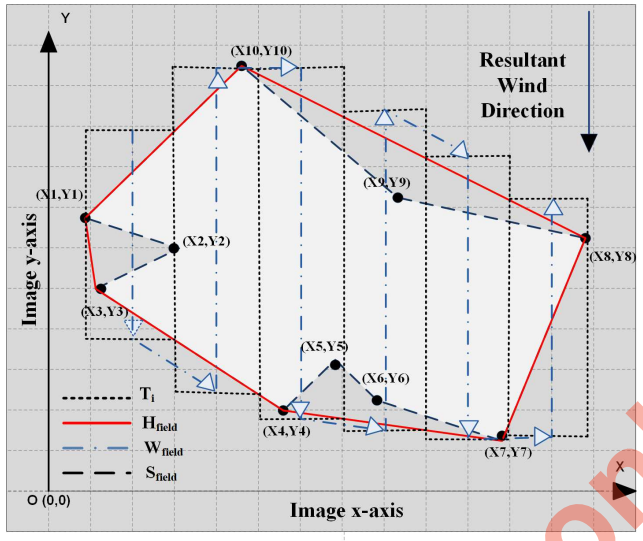

Fig. 8. Convex hull of detected field and implementing path planning

T_i can be generalized as,

$$\begin{aligned} T_i = \Bigg[& \left(x_{min} + (i-1)D_s, y_p + \frac{y_p - y_{p+1}}{x_p - x_{p+1}}(x_{min} + (i-1)D_s - x_p)\right), \\ & \left(x_{min} + (i-1)D_s, y_q + \frac{y_q - y_{q+1}}{x_q - x_{q+1}}(x_{min} + (i-1)D_s - x_q)\right), \\ & \left(x_{min} + iD_s, y_m + \frac{y_m - y_{m+1}}{x_m - x_{m+1}}(x_{min} + iD_s - x_m)\right), \\ & \left(x_{min} + iD_s, y_n + \frac{y_n - y_{n+1}}{x_n - x_{n+1}}(x_{min} + iD_s - x_n)\right)\Bigg] \\ & = [(T_{i1_x}, T_{i1_y}), (T_{i2_x}, T_{i2_y}), (T_{i3_x}, T_{i3_y}), (T_{i4_x}, T_{i4_y})] \\ & \text{where } i = 1, 2, 3, \ldots \end{aligned} \tag{16}$$

T_i is referred in Fig. 8. The way-point map for the UAV to traverse the H_{field} is defined as,

$$\begin{aligned} W_{field} = & \{W_1, W_2, W3, \ldots. W_i, ..\} \text{ where} \\ & W_i = \Big\{(\frac{T_{i2_x} + T_{i4_x}}{2}, max\{T_{i2y}, T_{i4y}\}), (\frac{T_{i1_x} + T_{i3_x}}{2}, \\ & min\{T_{i1y}, T_{i3y}\}\Big\} \\ & W_{i+1} = \Big\{(\frac{T_{(i+1)2_x} + T_{(i+1)4_x}}{2}, min\{T_{(i+1)2y}, T_{(i+1)4y}\}), \\ & (\frac{T_{(i+1)1_x} + T_{(i+1)3_x}}{2}, max\{T_{(i+1)1y}, T_{(i+1)3y}\}\Big\} \end{aligned} \tag{17}$$

W_{field} is the generated way-point map for the UAV, which ensures efficient coverage of the target field. The evaluation process of W_{field} and the implementation of path planning on it are shown in Fig. 8.

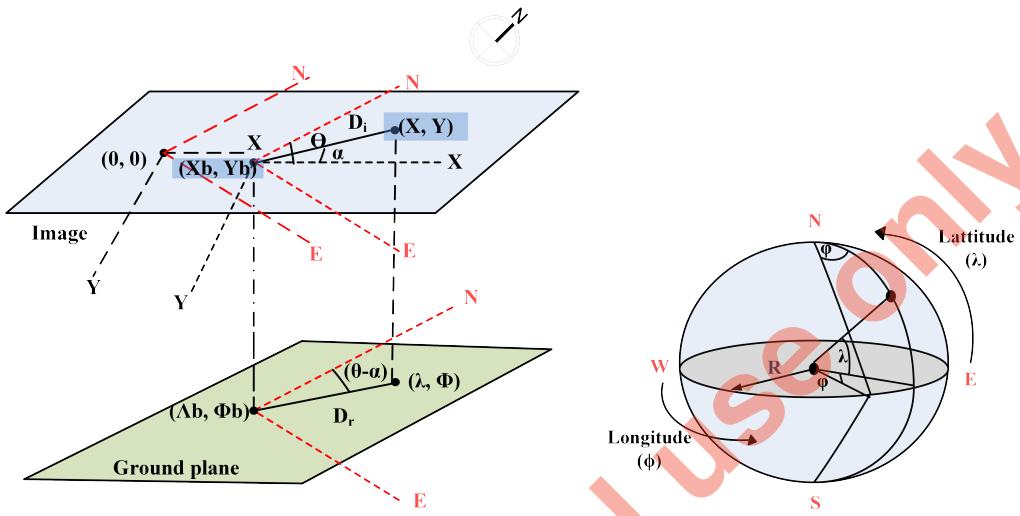

(a) Placement of image distance to real distance with respect to geometric North

(b) Measurement of latitude and longitude

Fig. 9. Image co-ordinate to GPS co-ordinate conversion

4.4 Marker Geo-Tagging and Pixel Way-point Map Generation

The final image captured by the UAV is processed to determine the geographic location of the marker and create a pixel waypoint map of the entire field detected in the image. An error-free geo-tagging and subsequent map generation is ensured by adjusting the camera mounted on the UAV such that it has no tilt during flight. Furthermore, to ease the calculation, an assumption is taken that all points on the agricultural field have the same altitude and equals to zero. The points in W_{field} are converted to corresponding GPS way-point map G_{field}. The autonomous UAV follows the generated way-point map.

Let θ be the angle between image x-axis and geometric north in counterclockwise direction. Any point in W_{field} (x, y) can be converted into the corresponding GPS location (ϕ, λ) using the location of the marker (ϕ_b, λ_b) as reference.

The GPS location of the marker (ϕ_b, λ_b) is evaluated as,

$$\begin{aligned}\left\{\phi_b, \lambda_b\right\} = \Bigg\{\phi_f + \frac{D_b \cos(\theta - \alpha)}{R} = \\ \phi_f + \frac{2H\sqrt{(x_b - \frac{p}{2})^2 + (y_b - \frac{q}{2})^2}}{R\sqrt{p^2 + q^2}} \\ \tan\frac{\beta}{2}\cos(\theta - \tan^{-1}\frac{y_b - \frac{q}{2}}{\frac{p}{2} - x_b}), \\ \lambda_f + \frac{D_b \cos(90^0 - \theta + \alpha)}{R} = \\ \lambda_f + \frac{2H\sqrt{(x_b - \frac{p}{2})^2 + (y_b - \frac{q}{2})^2}}{R\sqrt{p^2 + q^2}} \\ \tan\frac{\beta}{2}\sin(\theta - \tan^{-1}\frac{y_b - \frac{q}{2}}{\frac{p}{2} - x_b})\Bigg\}\end{aligned} \tag{18}$$

The value of θ comes from the reading of the compass mounted on the UAV processor board. The value (ϕ_f, λ_f) is the GPS location of the UAV. The change in latitude is measured from the angular displacement towards geometrical north and change in longitude is defined as angular displacement towards the geometrical east as referred in Fig.9(b). So, the corresponding GPS location of the image coordinate (X, Y) is calculated as:

$$\begin{aligned}\phi &= \phi_b + \frac{D_r \cos(\theta - \alpha)}{R} \\ &= \phi_b + \frac{2H\sqrt{(x - x_b)^2 + (y - y_b)^2}\tan\frac{\beta}{2}\cos(\theta - \tan^{-1}\frac{y_b - y}{x - x_b})}{R\sqrt{p^2 + q^2}}\end{aligned} \tag{19}$$

$$\begin{aligned}\lambda &= \lambda_b + \frac{D_r \cos(90^0 - \theta + \alpha)}{R} \\ &= \lambda_b + \frac{2H\sqrt{(x - x_b)^2 + (y - y_b)^2}\tan\frac{\beta}{2}\sin(\theta - \tan^{-1}\frac{y_b - y}{x - x_b})}{R\sqrt{p^2 + q^2}}\end{aligned} \tag{20}$$

5 RESULTS

An experimental trial was conducted in the agricultural fields of the Agricultural Department, Indian Institute of Technology, Kharagpur, India. The field is divided into smaller sub-fields with well-defined boundaries. A random crop field was selected and a marker was placed inside one of the sub-fields. An approximate GPS location of the selected sub-field was provided to the UAV as the initial location. A hand-held wind vane was used to determine the direction of the wind flow and place the UAV accordingly. After the initiation of the mission, the UAV reached the manually fed approximate GPS location of the field and followed the process described in the methodology section.

5.1 Area Covering Efficiency in Boundary Detection

While the area of the detected field is calculated efficiently, it is seen that the efficiency increases with the increase in the altitude of the UAV. With the increasing altitude, the captured image contains a better view and complete coverage of the field, thereby reducing any chances of loss of information. The formation of the convex hull makes the detection

Algorithm 3 Geo-Mapping

Inputs: $\lambda_b \rightarrow$ Marker latitude
$\phi_b \rightarrow$ Marker longitude
H $\rightarrow$ UAV altitude
R $\rightarrow$ Earth Radius
$p \times q \rightarrow$ Image-Sensor resolution of visual sensor used
$\beta \rightarrow$ Diagonal FoV of image sensor
$\theta \rightarrow$ Angle between geometric north and image x-axis

Output: GPS map of field $\rightarrow G_{field}$

$x_b \rightarrow X_c, y_b \rightarrow Y_c$
for p in W_{field} **do**
    p$\rightarrow (x, y)$
    $\alpha \rightarrow \tan^{-}1 \frac{y_b - y}{x - x_b}$
    Evaluate ϕ from eqn.19 and λ from eqn.20 using λ_b,ϕ_b,H,R,θ,α,β,p,q
    include $(\lambda, \phi) \rightarrow G_{field}$
end for

better by compensating the errors due to concave curvature. The detected boundary areas and original field areas are compared, the result of which is shown in Fig. 10. The average percentage efficiency of area coverage for varying

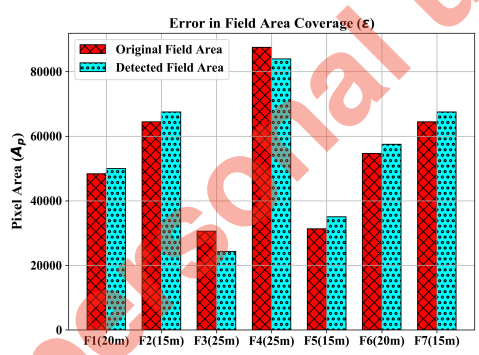

Fig. 10. Area coverage efficiency for different target fields

agricultural field is found to be 95.39%.

5.2 Marker Detection

The image is captured continuously until the marker is detected in the image. The detection is based on filtering the blue channel pixel values of the marker in the image. As the marker used is the same for all the fields, the blue channel values are the same for every detection. A common region of blue channel pixel value is used for marker detection. Fig.11 demonstrates the detection of a marker by the UAV at different altitudes. Fig.12 shows the common range of blue channel values for the marker used in the aerial images of the field. The vertical lines show the range of the pixel

(a) 15m Altitude (b) 20m Altitude (c) 25 m Altitude

Fig. 11. Marker detection and geo-tagging from aerial image

intensity peaks obtained for the detected blue beacon. The horizontal line separates the pixels with actual blue beacon from the rest of the image pixels containing other objects.

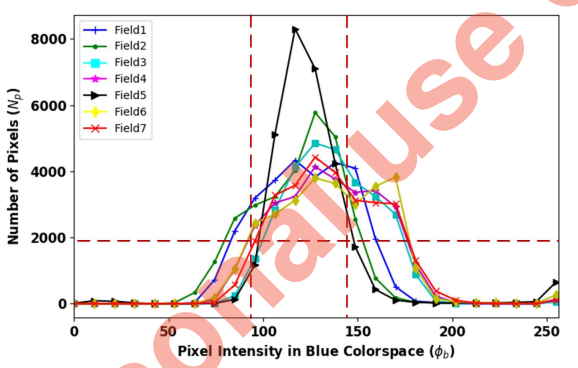

Fig. 12. Blue channel histogram plots for fields

5.3 Geo-tagging efficiency

The GPS location of the marker is calculated using Equations (19) and (20). The calculated GPS-coordinate of the marker is then compared with an android application based GPS reading of the location of the marker, taken on the spot. The comparison is shown in Fig. 13. At higher altitudes, the error is relatively lower. The error in calculation of GPS coordinates is due to the fact that the assumptions 1 and 2 mentioned in Equation 1 is not satisfied all the time.

The average absolute error in calculated latitude and longitude of the marker is 0.000107 degrees and 0.000044 degrees, respectively.

5.4 Coverage Efficiency of SDRWF approach

The SDRWF approach of path planning is applied on several aerial images of the fields. Some area outside the field is covered during path traversal, leading to loss of energy. The loss increases for a higher value of D_s. The increase in the value of D_s can be attributed to a larger value of the sensor footprint or a smaller overlap strip consideration. A larger

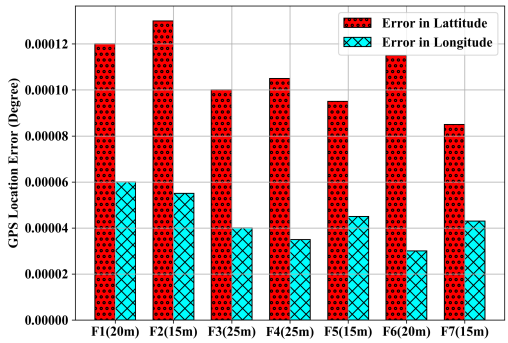

Fig. 13. Geo-tagging error for marker

sensor footprint will result into a larger area coverage during a single strip traversal, eventually leading to increased loss in the form of unwanted coverage. A comparative plot of area covered by UAV outside target field (ϵ) for different values of D_s is shown in Fig. 14.

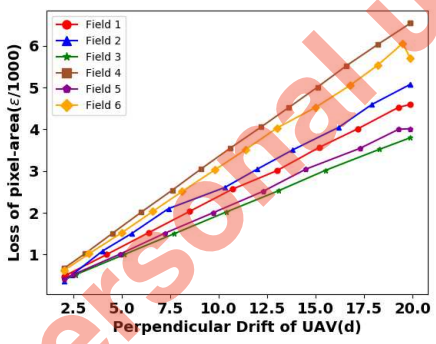

Fig. 14. ϵ vs D_s for different fields

5.5 Path Planning Implementation

The way-point map for path traversal over the field is converted into GPS map using pixel to GPS coordinate conversion, implemented using Algorithm 3. This way-point map is followed by the UAV to efficiently cover the detected field. Fig. 15 shows the implementation of SDRWF approach on aerial images of the fields.

5.6 Comparison with Existing Approaches

We compare the proposed path planning approach, SDRWF, with the existing path planning methods discuss in Section 4.3. The results are compared in terms of the number of turns by the UAV, distance travelled by UAV during the traversal, and the additional area covered by the UAV outside the target land. The proposed approach achieves minimum number

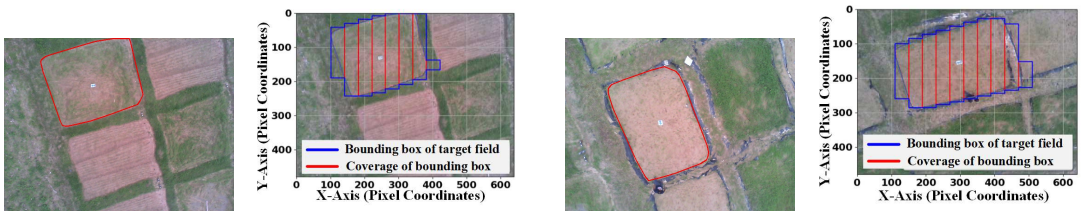

(a) Detection of field 1 (b) Path-planninng on field 1 (c) Detection of field 2 (d) Path-planning on field 2

Fig. 15. Path-planning on real field-images in SDRWF approach

of turns by UAV as compared to the other existing methods. While the IECD and ZigZag approach result in maximum number of turns for all the target fields, shown in Fig. 16. The minimum number of turns in the proposed approach ensures that minimum information is lost in the form of parts of the target land that remain uncovered during its traversal. In terms of the distance covered by the UAV during traversal, the proposed approach performs better than the Zamboni and Lawnmower approach, shown in Fig. 17. However, the distance travelled by UAV using IECD, Spiral, and ZigZag approches exhibit minimum distance traversal. In SDRWF the sweep occurs along the resultant wind flow direction instead of along the optimal sweep. This ensures smaller deviation of UAV from the planned path or waypoint. In case of small deviations due to a sudden change in wind direction, the initial overlap of $2\delta_s$ compensates it, as shown in the Fig. 7(b). Fig. 18 shows the area covered outside the target field during traversal. The area covered outside the target field by UAV is higher in the proposed approach as compared to the other compared approaches. This behaviour can be attributed to undesirable weather conditions. However the target field is covered with 100% coverage as visible in Fig. 15(b) and 15(b). The implementation of ZigZag approach in [3] shows an area coverage of approximately 80%. The proposed marker detection approach performs successfully at a maximum tested altitude of $25m$. A similar system using markers to detect a target land is implemented in [1] which is able to detect the target from distance of $5m$. Higher altitude enables the UAV to cover a larger area from its position.

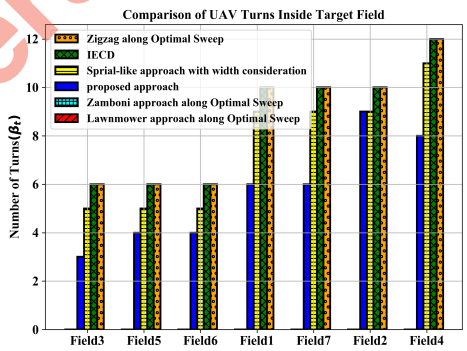

Fig. 16. Comparison of number of sharp turns by UAV inside target field.

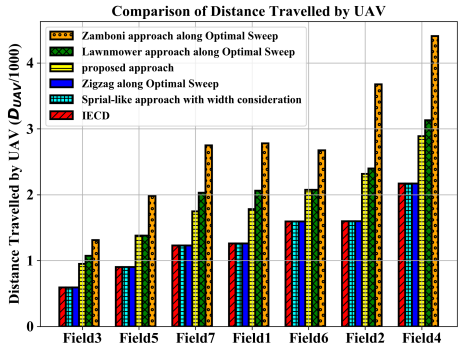

Fig. 17. Comparison of distance coverage by UAV.

6 CONCLUSION

The proposed system performs well, even under real-time implementation environments. It is capable of real-time target field detection and designing suitable path planning, even during loss of its connectivity to the base station. The detection and geo-tagging of the target field is performed onboard during the flight. This is followed by efficient path planning onboard. The successful conversion of pixel to GPS coordinates in real-time makes it convenient and flexible, thereby removing the dependencies on pre-installed offline GPS waypoint maps. The detection process performs even better for higher altitudes of UAV as the boundary of the target field becomes more prominent. The process is convenient for smaller fields due to the marker based detection method, thereby reducing the GPS error.

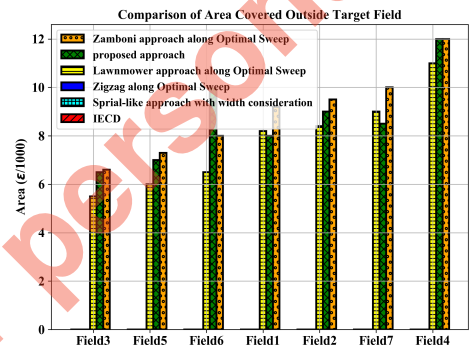

Fig. 18. Comparison of area coverage outside target field.

As a future scope, the detection process can be improved for detection of target fields with complex boundary and non-convex structure. Various other forms of marker may be introduced to make the marker detection more flexible. More efficient computer vision techniques can be used to replace the beacon-based detection approach. Some robust GPS error correction process can be included to further reduce the GPS error and accurately cover the field without loss of information or energy. More efficient field coverage methods can be implemented, considering the resource

constraints in UAV. The presented approach can also be applied in networks of UAVs with further modifications and enhancement.

REFERENCES

[1] Bilal Hazim Younus Alsalam, Kye Morton, Duncan Campbell, and Felipe Gonzalez. 2017. Autonomous UAV with vision based on-board decision making for remote sensing and precision agriculture. In *IEEE Aerospace Conference*. 1–12.

[2] JF Araujo, PB Sujit, and João B Sousa. 2013. Multiple UAV area decomposition and coverage. In *IEEE Symposium on Computational Intelligence for Security and Defense Applications (CISDA)*. 30–37.

[3] Evander Christy, Rina Pudji Astuti, Budi Syihabuddin, Bhaskara Narottama, Obed Rhesa, and Furry Rachmawati. 2017. Optimum UAV flying path for device-to-device communications in disaster area. In *2017 International Conference on Signals and Systems (ICSigSys)*. IEEE, 318–322.

[4] Fausto G Costa, Jó Ueyama, Torsten Braun, Gustavo Pessin, Fernando S Osório, and Patrícia A Vargas. 2012. The use of unmanned aerial vehicles and wireless sensor network in agricultural applications. In *IEEE International Geoscience and Remote Sensing Symposium (IGARSS)*. 5045–5048.

[5] Sophie Crommelinck, Rohan Bennett, Markus Gerke, Michael Ying Yang, and George Vosselman. 2017. Contour Detection for UAV-Based Cadastral Mapping. *Remote Sensing* 9 (02 2017), 171.

[6] O. Esrafilian and D. Gesbert. 2017. 3D City Map Reconstruction from UAV-Based Radio Measurements. In *Proceedings of the IEEE Global Communications Conference*. 1–6.

[7] Bruno S Faical, Jo Ueyama, and Andre CPLF de Carvalho. 2016. The use of autonomous UAVs to improve pesticide application in crop fields. In *Proceedings of the 17th IEEE International Conference on Mobile Data Management (MDM)*, Vol. 2. 32–33.

[8] Ayman Habib, Weifeng Xiong, Fangning He, Hsiuhan Lexie Yang, and Melba Crawford. 2017. Improving Orthorectification of UAV-Based Push-Broom Scanner Imagery Using Derived Orthophotos From Frame Cameras. *IEEE Journal of Selected Topics in Applied Earth Observations and Remote Sensing* 10, 1 (2017), 262–276.

[9] Faez M Hassan, MZ Mat Jafri, and HS Lim. 2011. Contextual classification of cropcam uav high resolution images using frequency-based approach for land use/land cover mapping case study: Penang island. In *IEEE Symposium on Industrial Electronics and Applications (ISIEA)*. 663–668.

[10] Yu-Song Jiao, Xin-Min Wang, Hai Chen, and Yan Li. 2010. Research on the coverage path planning of uavs for polygon areas. In *Proceedings of the 5th IEEE Conference on Industrial Electronics and Applications (ICIEA)*. 1467–1472.

[11] Wei Li, Haidi Yuan, and Liangtu Song. 2016. Prediction of wheat gains with imagery from four-rotor UAV. In *Proceedings of the 2nd IEEE International Conference on Computer and Communications (ICCC)*. 662–665.

[12] Huilin Liang, Weizheng Li, Qingping Zhang, Wen Zhu, Di Chen, Jie Liu, and Ting Shu. 2017. Using unmanned aerial vehicle data to assess the three-dimension green quantity of urban green space: A case study in Shanghai, China. *Landscape and Urban Planning* 164 (2017), 81 – 90.

[13] Mohamad Farid Misnan, Nor Hashim Mohd Arshad, Ruhizan Liza Ahmad Shauri, Noorfadzli Abd Razak, Norashikin Mohd Thamrin, and Siti Fatimah Mahmud. 2013. Real-time vision based sensor implementation on unmanned aerial vehicle for features detection technique of low altitude mapping. In *Proceedings of the IEEE Conference on Systems, Process & Control (ICSPC)*. 289–294.

[14] M. R and R.K. R. 1998. *Moment Functions In Image Analysis - Theory And Applications*. World Scientific Publishing Company.

[15] Sheilla Ayu Ramadhani, R. M. Bennett, and F. C. Nex. 2018. Exploring UAV in Indonesian cadastral boundary data acquisition. *Earth Science Informatics* 11, 1 (01 Mar 2018), 129–146.

[16] Temuulen T. Sankey, Jason McVay, Tyson L. Swetnam, Mitchel P. McClaran, Philip Heilman, Mary Nichols, Nathalie Pettorelli, and Ned Horning. 2017. UAV hyperspectral and lidar data and their fusion for arid and semi-arid land vegetation monitoring. *Remote Sensing in Ecology and Conservation* 4, 1 (2017), 20–33.

[17] Daniela Stroppiana, Mauro Migliazzi, Valter Chiarabini, Alberto Crema, Mauro Musanti, Carlo Franchino, and Paolo Villa. 2015. Rice yield estimation using multispectral data from UAV: A preliminary experiment in northern Italy. In *IEEE International Geoscience and Remote Sensing Symposium (IGARSS)*. 4664–4667.

[18] Jinmika Wijitdechakul, Shiori Sasaki, Yasushi Kiyoki, and Chawan Koopipat. 2016. UAV-based multispectral image analysis system with semantic computing for agricultural health conditions monitoring and real-time management. In *IEEE International Electronics Symposium (IES)*. 459–464.